

Point2RBox-v2: Rethinking Point-supervised Oriented Object Detection with Spatial Layout Among Instances

Yi Yu^{1*}, Botao Ren^{2*}, Peiyuan Zhang^{3*}, Mingxin Liu⁴, Junwei Luo³, Shaofeng Zhang⁴,
Feipeng Da¹, Junchi Yan⁴, Xue Yang^{4†}

¹Southeast University ²Tsinghua University ³Wuhan University ⁴Shanghai Jiao Tong University

{yuyi,dafp}@seu.edu.cn rbt22@mails.tsinghua.edu.cn {peiyuanzhangwhu,luojunwei}@whu.edu.cn

{liumingxin,zhangshaofeng,yanjunchi,yangxue-2019-sjtu}@sjtu.edu.cn

<https://github.com/VisionXLab/point2rbox-v2>

Abstract

With the rapidly increasing demand for oriented object detection (OOD), recent research involving weakly-supervised detectors for learning OOD from point annotations has gained great attention. In this paper, we rethink this challenging task setting with the layout among instances and present Point2RBox-v2. At the core are three principles: **1) Gaussian overlap loss.** It learns an upper bound for each instance by treating objects as 2D Gaussian distributions and minimizing their overlap. **2) Voronoi watershed loss.** It learns a lower bound for each instance through watershed on Voronoi tessellation. **3) Consistency loss.** It learns the size/rotation variation between two output sets with respect to an input image and its augmented view. Supplemented by a few devised techniques, e.g. edge loss and copy-paste, the detector is further enhanced. To our best knowledge, Point2RBox-v2 is the first approach to explore the spatial layout among instances for learning point-supervised OOD. Our solution is elegant and lightweight, yet it is expected to give a competitive performance especially in densely packed scenes: 62.61%/86.15%/34.71% on DOTA/HRSC/FAIR1M.

1. Introduction

Emerged as an essential task in computer vision, oriented object detection (OOD) has become a prominent demand in autonomous driving [6], aerial images [7, 30, 48, 51, 52], scene text [23, 28, 71], retail scenes [10, 35], industrial inspection [29, 47], and more.

Manual annotations are essential to teach the detector new concepts of visual objects. Early research is often super-

*Equal contribution. †Corresponding author. The work was partly supported by National Natural Science Foundation of China (62306069, 62222607, 72342023), China Postdoctoral Science Foundation (2023M740602), National Key R&D Program of China (2022ZD0160100), Jiangsu Funding Program for Excellent Postdoctoral Talent (2023ZB616).

PointOBB	😊 Multiple instance learning	30.08	Pseudo generator
PointOBB-v2	😊 Class probability map	44.90	
PointOBB-v3	😊 Multiple instance learning	49.24	
P2RBox	😞 Pre-trained SAM (prior)	59.04	End-to-end
Point2RBox-v2 (ours)	😊 Layout among instances	62.61	
PointOBB-v3	😊 Multiple instance learning	41.29	
Point2RBox	😞 One-shot examples (prior)	40.27	End-to-end
	😊 Knowledge from synthetic	34.07	

Figure 1. Related methods, their principles for knowledge mining, whether using additional priors, and performance on DOTA-v1.0.

vised by rotated bounding boxes (RBoxes), where annotations align with the desired output. While this approach has demonstrated promising results, RBox labels are considerably expensive. The cost of annotating each RBox is approximately 36.5% higher than a horizontal bounding box (HBox) and 104.8% higher than a point [66]. This highlights the importance of utilizing coarser labels for weakly-supervised oriented detection. Recent advancements in HBox-supervised OOD, particularly with H2RBox [59] and H2RBox-v2 [65], have shown promise in bridging the gap between HBox- and RBox-supervised methods, thereby lessening the dependence on labor-intensive RBox labeling.

Following HBox-supervised methods, the more challenging point-supervised OOD opens up a new avenue. Several innovative approaches have emerged in the past year (see Fig. 1): **1) Point-prompt OOD.** P2RBox [2], PMHO [68], and PointSAM [27] employ the zero-shot ability of SAM [17]. **2) Pseudo generation.** PointOBB [33] and its v2/v3 version [38, 67] use multiple instance learning and class probability map for RBox generation. **3) Knowledge combination.** Point2RBox [66] learns from one-shot examples. However, existing methods overlook the spatial relationships between objects. This brings us to the motivation of this paper.

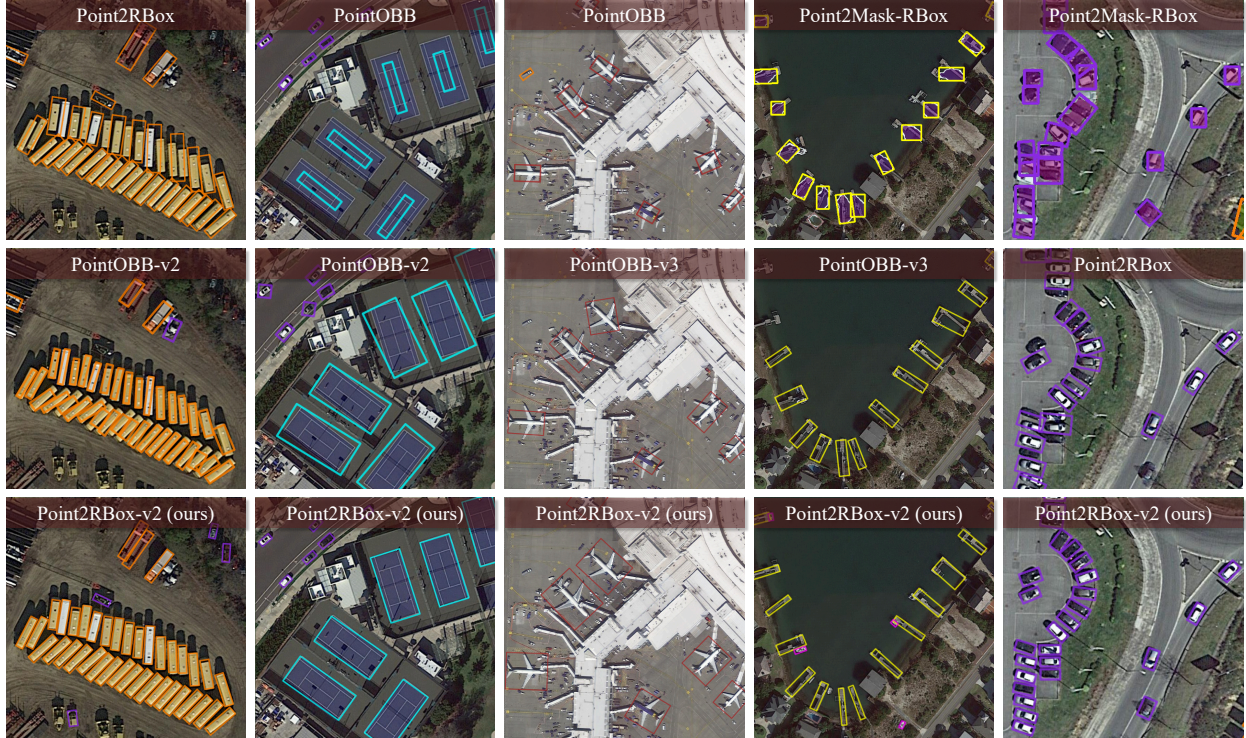


Figure 2. Visual comparisons with state-of-the-art methods including: Point2Mask (2023) [21], PointOBB (2024) [33], PointOBB-v2 (2025) [38], PointOBB-v3 (2025) [67], and Point2RBox (2024) [66]. The boxes detected by our method (last row) wrap the objects more tightly.

Motivation. While point-supervised OOD has gained attention, the utilization of relationships among instances remains absent in the literature. For example, the arrangement of vehicles in a parking lot can serve as effective constraints for learning their size and orientation. This approach may yield valuable insights into point-supervised OOD, particularly in densely packed scenes where current methods face significant challenges. Can we leverage the spatial layout of objects to enhance point-supervised OOD? In this paper, we dive into this idea and seek to answer this question.

Highlights. **1)** Point2RBox-v2 is proposed for point-supervised OOD, advancing the state of the art as displayed in Fig. 2 and Tables 1-2. **2)** We propose novel and elegant losses to enforce constraints from the spatial layout among instances based on Gaussian overlap and Voronoi tessellation [1]. **3)** Other modules are devised (i.e. edge loss, consistency loss, copy-paste) to further enhance the method.

Contributions. **1)** To our best knowledge, this work is the first attempt to learn point-supervised OOD from the layout among objects, where we propose novel principles based on Gaussian overlap and Voronoi tessellation. **2)** The training pipeline and detailed implementation are elucidated, with necessary modules (i.e. edge loss, consistency loss, copy-paste) incorporated. The source code will be made publicly available. **3)** Extensive experiments demonstrate that leveraging the spatial layout of instances can significantly advance the state of the art, surpassing other alternatives in accuracy.

2. Related Work

2.1. RBox-supervised Oriented Detection

In addition to horizontal detection [26, 70], oriented object detection (OOD) [46, 52] has received extensive attention. Representative works include anchor-based detector Rotated RetinaNet [25], anchor-free detector Rotated FCOS [42], and two-stage solutions, e.g. RoI Transformer [5], Oriented R-CNN [49], and ReDet [11]. Some research enhances the detector by exploiting alignment features, e.g. R³Det [55] and S²A-Net [12]. The angle regression may face boundary discontinuity and remedies are developed, including modulated losses [37, 53, 58] that alleviate loss jumps, angle coders [50, 51, 54, 63] that convert the angle into boundary-free coded data, and Gaussian-based losses [34, 56, 57, 60, 61] transforming rotated bounding boxes into Gaussian distributions. RepPoint-based methods [15, 20, 62] provide alternatives that predict a set of points that bounds the spatial extent of an object. LMMRotate [19] is a new paradigm of OOD based on multimodal language model and performs object localization through autoregressive prediction.

2.2. Point-supervised Oriented Detection

Recently, several methods for point-supervised oriented detection have been proposed: **1)** P2RBox [2], PMHO [68], and PointSAM [27] propose oriented detection with point prompts by employing the zero-shot Point-to-Mask ability

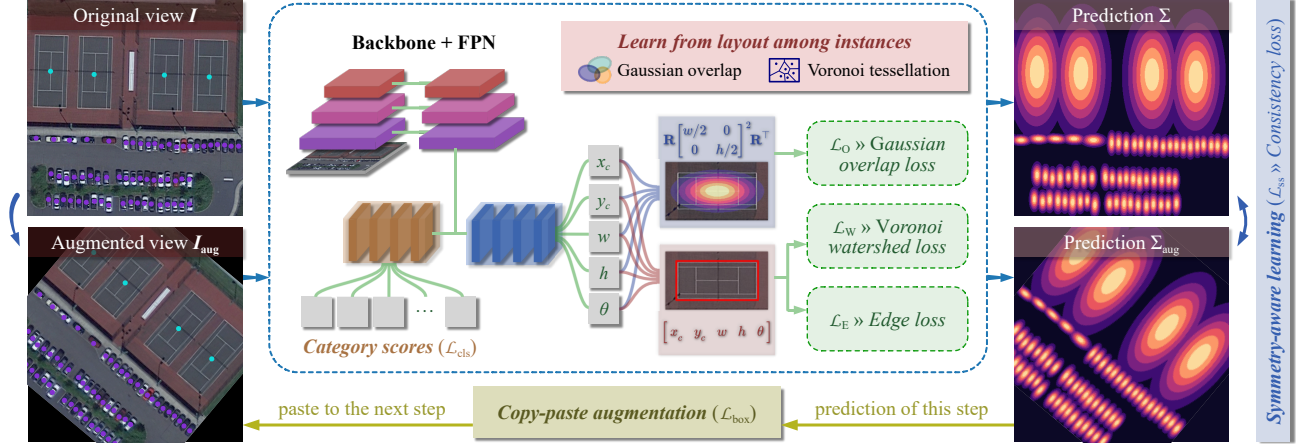


Figure 3. The training pipeline of Point2RBox-v2. Gaussian overlap loss and Voronoi watershed loss utilize the spatial layout (see Fig. 4), while edge loss (see Sec. 3.4), symmetry-aware learning (see Sec. 3.5), and copy-paste (see Sec. 3.6) further enhance the method.

of SAM [17]. 2) Point2RBox [66] introduces an end-to-end approach based on knowledge combination. 3) PointOBB [33, 67] achieves RBox generation through scale consistency and multiple instance learning. 4) PointOBB-v2 [38] learns a class probability map to generate pseudo RBox labels.

Among these methods, P2RBox, PMHO, and PointSAM rely on the SAM model pre-trained on massive labeled datasets, whereas Point2RBox requires one-shot examples for each category. In contrast, PointOBB series do not use many priors, but they necessitate two-stage training.

2.3. Other Weakly-supervised Settings

Compared to Point-to-RBox, some other settings have been better studied. These methods are potentially applicable to our Point-to-RBox task setting by using a cascade pipeline, such as Point-to-HBox-to-RBox. In our experiment, cascade pipelines powered by state-of-the-art approaches are also compared. Here, representative works are introduced.

HBox-to-RBox. H2RBox [59] establishes a paradigm that limits the object to a few candidate angles through geometric constraint from HBoxes, with a self-supervised branch eliminating the undesired results. An enhanced version H2RBox-v2 [65] is proposed to leverage the reflection symmetry of objects to further boost the accuracy. EIE-Det [45] uses an explicit equivariance branch for learning rotation consistency, and an implicit equivariance branch for learning position, aspect ratio, and scale consistency. KCR [73] combines RBox- and HBox-annotated datasets for transfer learning. Some studies [16, 41] use additional annotated data for training, which are also attractive but less general.

Point-to-HBox. Several related approaches have been developed, including: 1) P2BNet [3] samples box proposals of different sizes around the labeled point and classify them to achieve point-supervised horizontal object detection. 2) PSOD [8] achieves point-supervised salient object detection using an edge detector and adaptive masked flood fill.

Point-to-Mask. Point2Mask [21] is proposed to achieve panoptic segmentation using single point annotation per target. SAM (Segment Anything Model) [17] produces object masks from input point/HBox prompts. Though RBoxes can be obtained from the segmentation mask by finding the minimum circumscribed rectangle, such a complex pipeline can be less cost-efficient and perform worse [59, 65].

3. Method

3.1. Overview and Preliminary

An overview of Point2RBox-v2 is illustrated in Fig. 3. The network is based on ResNet50 [13] backbone, FPN [24] head, and PSC [64] angle coder. Objects of varying sizes are typically assigned to different FPN layers based on the scale. However, points lack size, so we assign them all to the P3 layer (stride = 8). Assume the detector $f_{nn}(\cdot)$ maps an image I to a set of RBoxes as detection results:

$$(x_c, y_c, w, h, \theta) = f_{nn}(I) \quad (1)$$

Equivalently, oriented objects can also be represented by 2D Gaussian distributions $\mathcal{N}(\mu, \Sigma)$ [60]:

$$\left\{ \mu = [x_c \ y_c], \quad \Sigma = \mathbf{R} \begin{bmatrix} w/2 & 0 \\ 0 & h/2 \end{bmatrix}^2 \mathbf{R}^\top \right\} \quad (2)$$

where

$$\mathbf{R} = \begin{bmatrix} \cos \theta & -\sin \theta \\ \sin \theta & \cos \theta \end{bmatrix} \quad (3)$$

At the core of Point2RBox-v2 is to utilize the constraints from the layout, which is achieved by Gaussian overlap loss (Sec. 3.2) and Voronoi watershed loss (Sec. 3.3). These two losses effectively limit the size and rotation of objects to a reasonable range. Upon that, edge loss (Sec. 3.4) aligns the bounding box with the edge of objects to improve the accuracy. Incorporated with symmetry-aware learning (Sec. 3.5) and copy-paste augmentation (Sec. 3.6), we achieve a

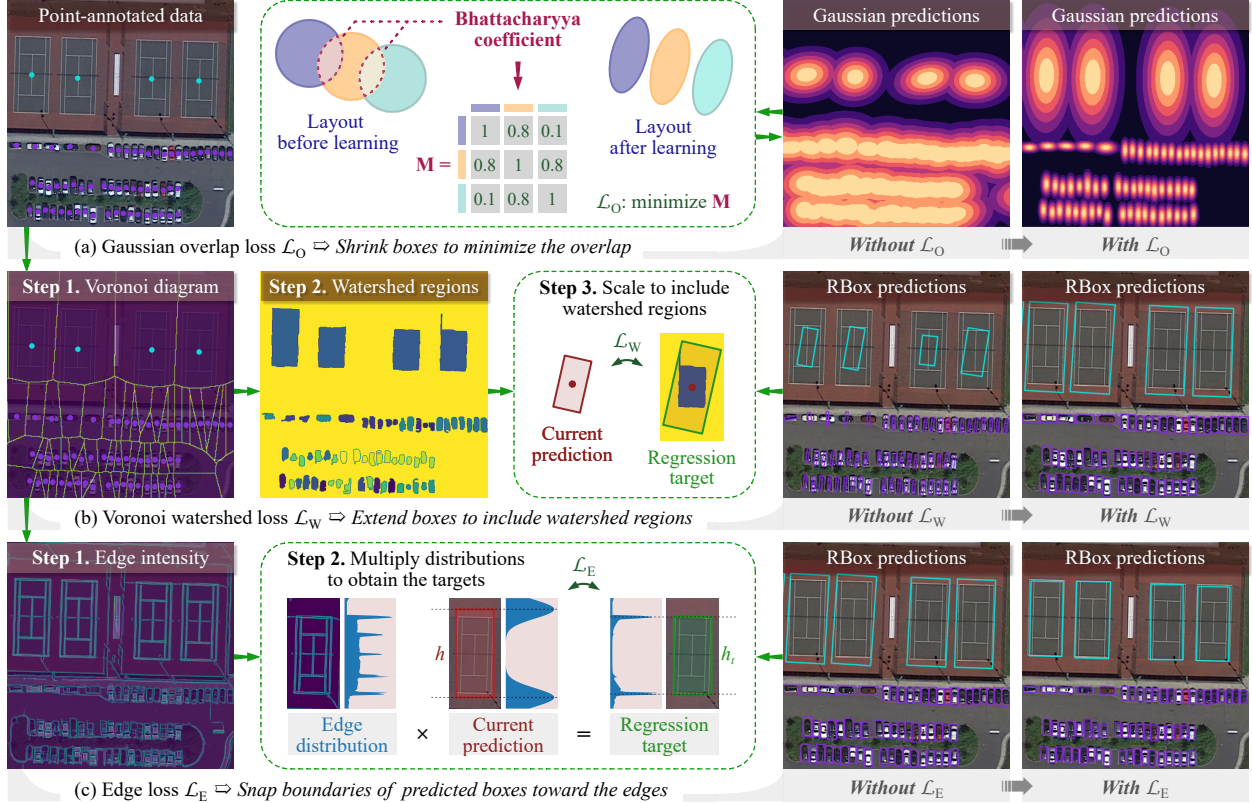


Figure 4. To illustrate the procedure of the three newly proposed loss functions and their impact on the learning results. (a) Gaussian overlap loss (see Sec. 3.2). (b) Voronoi watershed loss (see Sec. 3.3). (c) Edge loss (see Sec. 3.4).

stable and high-accuracy solution for point-supervised OOD. In subsequent subsections, these modules are detailed.

3.2. Gaussian Overlap Loss

As mentioned, oriented objects can be represented by 2D Gaussian distributions $\mathcal{N}(\mu, \Sigma)$. The overlap volume between two distributions $\mathcal{N}_1(\mu_1, \Sigma_1)$ and $\mathcal{N}_2(\mu_2, \Sigma_2)$ can be approximated by the Bhattacharyya coefficient [60] as:

$$B(\mathcal{N}_1, \mathcal{N}_2) = \exp\left(-\frac{1}{8}\mu^\top \Sigma^{-1}\mu\right) \cdot \frac{|\Sigma_1|^{1/4} |\Sigma_2|^{1/4}}{|\Sigma|^{1/2}} \quad (4)$$

where $\mu = \mu_2 - \mu_1$, $\Sigma = \frac{1}{2}(\Sigma_1 + \Sigma_2)$, $|\Sigma|$ denotes the determinant of the covariance matrix.

Based on the above equation, we build a Gaussian overlap matrix $\mathbf{M} \in \mathbb{R}^{N \times N}$ for each scene image as:

$$\mathbf{M}_{i,j} = B(\mathcal{N}_i, \mathcal{N}_j) \quad (5)$$

where $i, j = 1, 2, \dots, N$; N is the distribution count (or the instance count) within one training image.

The Gaussian overlap loss can then be expressed as:

$$\mathcal{L}_O = \frac{1}{N} \sum_{i \neq j} (\mathbf{M}_{i,j}) \quad (6)$$

where $i \neq j$ omits diagonal elements. With this loss, the

detector learns to arrange instances (see Fig. 4a) based on the mutual exclusivity among instances.

3.3. Voronoi Watershed Loss

A Voronoi diagram [1] is a partitioning of a space based on a set of points. Point annotations can be effectively utilized to calculate a Voronoi diagram, where a distinct polygon region is assigned to each point-annotated instance. The watershed algorithm [44], on the other hand, is a region segmentation technique that treats the intensity of pixels as a topographic surface, identifying regions as ‘‘catchment basins’’.

The calculation of Voronoi ridges can be formulated as:

$$V = \text{Voronoi}(X) \quad (7)$$

where X are the annotated points within a training image; V are the output Voronoi ridges (pixel coordinates).

Interestingly, we find that Voronoi diagrams can be utilized as initial markers for watershed to obtain a region for each instance (see Fig. 4b). In concrete terms, the points X can be employed as foreground markers, while the Voronoi ridges V can act as background boundaries:

$$S = \text{Watershed}(I, X, V) \quad (8)$$

where S are the output basin regions (pixel coordinates) corresponding to each annotated instance. By rotating S

to align with the direction of the current prediction, the regression target of width and height can be expressed as:

$$\begin{bmatrix} w_t \\ h_t \end{bmatrix} = 2 \max \left| \mathbf{R}^\top \left(S - \begin{bmatrix} x_c \\ y_c \end{bmatrix} \right) \right| \quad (9)$$

where (x_c, y_c, w, h, θ) is the current prediction; \mathbf{R} is defined by Eq. (3); w_t and h_t are detached to stop the gradient.

Afterward, the Voronoi watershed loss to regress the width and height of objects can be calculated as:

$$\mathcal{L}_W = L_{\text{GWD}} \left(\begin{bmatrix} w/2 & 0 \\ 0 & h/2 \end{bmatrix}^2, \begin{bmatrix} w_t/2 & 0 \\ 0 & h_t/2 \end{bmatrix}^2 \right) \quad (10)$$

where $L_{\text{GWD}}(\cdot)$ is Gaussian Wasserstein Distance Loss [60].

3.4. Edge Loss

The above two losses have limited the size to a reasonable range. To make it more accurate, we propose the edge loss to snap the boundaries toward the edges (see Fig. 4c).

First, a region $P \in \mathbb{R}^{(2K+1) \times (2K+1)}$ around each predicted RBox is extracted via Rotated RoI Align [14]:

$$P = \text{RoIAlign}(E(I), (x_c, y_c, \beta w, \beta h, \theta)) \quad (11)$$

where $E(\cdot)$ is the edge detection function [39]. We set $K = 24$ and $\beta = 1.6$ in our experiments (see Table 9).

By calculating the sum of each row of P , the edge distribution in y direction can be obtained as:

$$\mu_i = \sum_{j=1}^{2K+1} (P_{(K+1-i),j} + P_{(K+1+i),j}) \quad (12)$$

where $i = 1, 2, \dots, K$, indicating that the upper half of P is reversed and added to the lower half.

Meanwhile, the current prediction of the edge can also be softened into a distribution as:

$$\lambda_i = \exp \left(-\frac{(i - K/\beta)^2}{2\sigma_E^2} \right) \quad (13)$$

where $i = 1, 2, \dots, K$; σ_E is set to 6. Note that we crop P based on the predicted RBox, thus λ is always the same.

Multiplying the two distributions yields the target:

$$h_t = \frac{\beta h}{K} \arg \max(\mu \times \lambda) \quad (14)$$

where h_t is the regression target of height. Likewise, the width target w_t is calculated along x direction.

The edge loss is then obtained as:

$$\mathcal{L}_E = \text{smooth}_{L1}([w \ h], [w_t \ h_t]) \quad (15)$$

Note that \mathcal{L}_W and \mathcal{L}_E merely refines the width and height of boxes, without involving the angle regression.

3.5. Symmetry-aware Learning

Proven effective in learning the rotation of objects [65], in this work, symmetry-aware learning is extended to Gaussian-

based OOD. In the left part of Fig. 3, the training image I is transformed (randomly selected from rotation, flip, and scale, see Table 7) to generate an augmented view as:

$$I_{\text{aug}} = \alpha I \quad (16)$$

where

$$\alpha = \begin{bmatrix} \cos \mathcal{R} & -\sin \mathcal{R} \\ \sin \mathcal{R} & \cos \mathcal{R} \end{bmatrix}^{p_1} \begin{bmatrix} 1 & 0 \\ 0 & -1 \end{bmatrix}^{p_2} \begin{bmatrix} s & 0 \\ 0 & s \end{bmatrix}^{p_3} \quad (17)$$

where $(p_1, p_2, p_3) = (1, 0, 0)$ when rotation is selected, $(0, 1, 0)$ when flip, $(0, 0, 1)$ when scale. \mathcal{R} and s are the random amount of rotation and scale, $s \in (0.5, 0.9)$.

By feeding both I and I_{aug} into the network, we obtain two sets of output Gaussian distributions and angles:

$$\begin{cases} (\Sigma, \theta) = f_{\text{nn}}(I) \\ (\Sigma_{\text{aug}}, \theta_{\text{aug}}) = f_{\text{nn}}(I_{\text{aug}}) \end{cases} \quad (18)$$

The consistency loss is calculated between the two sets so that the network learns the size and rotation variation:

$$\mathcal{L}_{\text{ss}} = L_{\text{GWD}}(\alpha \Sigma \alpha^\top, \Sigma_{\text{aug}}) + L_{\text{ANG}}(m\theta + \mathcal{R}, \theta_{\text{aug}}) \quad (19)$$

where \mathcal{R} is the rotation angle and $m = 1$ when rotation is selected; $(m, \mathcal{R}) = (-1, 0)$ when flip; $(m, \mathcal{R}) = (1, 0)$ when scale. $L_{\text{GWD}}(\cdot)$ is Gaussian Wasserstein Distance Loss [60] and $L_{\text{ANG}}(\cdot)$ is defined as:

$$L_{\text{ANG}}(\theta_1, \theta_2) = \min_{k \in \mathbb{Z}} (\text{smooth}_{L1}(\theta_1, k\pi + \theta_2)) \quad (20)$$

where $\min(\cdot)$ regresses the prediction toward the closest target to circumvent the periodicity problem [65].

3.6. Copy-paste Augmentation

Inspired by [9], we propose to crop the detected instances of step k and paste them on the training image of step $k + 1$. The maximum number of paste boxes is limited to 10 in each step. We simply use the bounding boxes of the cropped instances as the regression targets, and use Gaussian Wasserstein Distance Loss [60] to calculate \mathcal{L}_{box} .

3.7. Overall Loss

The overall loss \mathcal{L} for Point2RBox-v2 can be expressed as:

$$\mathcal{L}_{\text{cls}} + w_{\text{box}} \mathcal{L}_{\text{box}} + w_{\text{O}} \mathcal{L}_{\text{O}} + w_{\text{W}} \mathcal{L}_{\text{W}} + w_{\text{E}} \mathcal{L}_{\text{E}} + w_{\text{ss}} \mathcal{L}_{\text{ss}} \quad (21)$$

where \mathcal{L}_{cls} is the focal loss [25] for classification, \mathcal{L}_{box} regresses boxes/centers toward copy-paste/ground-truth labels, w_{box} is set to one by default, $(w_{\text{O}}, w_{\text{W}}, w_{\text{E}}, w_{\text{ss}})$ are set to $(10, 5, 0.3, 1)$ based on our ablation studies (see Tables 3-5).

4. Experiments

Experiments are carried out on NVIDIA RTX4090 GPUs using PyTorch 2.2.0 [36] and the rotation detection tool kits: MMRotate 1.0.0 [72]. All the experiments follow the same hyper-parameters (learning rate, batch size, optimizer, etc.).

Methods	*	PL ¹	BD	BR	GTF	SV	LV	SH	TC	BC	ST	SBF	RA	HA	SP	HC	AP ₅₀
▼ <i>RBox-supervised OOD</i>																	
RepPoints (2019) [62]	✓	86.7	81.1	41.6	62.0	76.2	56.3	75.7	90.7	80.8	85.3	63.3	66.6	59.1	67.6	33.7	68.45
RetinaNet (2017) [25]	✓	88.2	77.0	45.0	69.4	71.5	59.0	74.5	90.8	84.9	79.3	57.3	64.7	62.7	66.5	39.6	68.69
GWD (2021) [56]	✓	89.3	75.4	47.8	61.9	79.5	73.8	86.1	90.9	84.5	79.4	55.9	59.7	63.2	71.0	45.4	71.66
FCOS (2019) [42]	✓	89.1	76.9	50.1	63.2	79.8	79.8	87.1	90.4	80.8	84.6	59.7	66.3	65.8	71.3	41.7	72.44
S ² A-Net (2022) [12]	✓	89.2	83.0	52.5	74.6	78.8	79.2	87.5	90.9	84.9	84.8	61.9	68.0	70.7	71.4	59.8	75.81
▼ <i>HBox-supervised OOD</i>																	
Sun et al. (2021) [41]	×	51.5	38.7	16.1	36.8	29.8	19.2	23.4	83.9	50.6	80.0	18.9	50.2	25.6	28.7	25.5	38.60
BoxInst-RBox (2021) [43] ²	×	68.4	40.8	33.1	32.3	46.9	55.4	56.6	79.5	66.8	82.1	41.2	52.8	52.8	65.0	30.0	53.59
H2RBox (2023) [59]	✓	88.5	73.5	40.8	56.9	77.5	65.4	77.9	90.9	83.2	85.3	55.3	62.9	52.4	63.6	43.3	67.82
EIE-Det (2024) [45]	✓	87.7	70.2	41.5	60.5	80.7	76.3	86.3	90.9	82.6	84.7	53.1	64.5	58.1	70.4	43.8	70.10
H2RBox-v2 (2023) [65]	✓	89.0	74.4	50.0	60.5	79.8	75.3	86.9	90.9	85.1	85.0	59.2	63.2	65.2	70.5	49.7	72.31
▼ <i>Point-supervised OOD</i>																	
Point2Mask-RBox (2023) [21] ²	×	4.0	23.1	3.8	1.3	15.1	1.0	3.3	19.0	1.0	29.1	0.0	9.5	7.4	21.1	7.1	9.72
P2BNet+H2RBox (2023) [3, 59]	×	24.7	35.9	7.1	27.9	3.3	12.1	17.5	17.5	0.8	34.0	6.3	49.6	11.6	27.2	18.8	19.63
P2BNet+H2RBox-v2 (2023) [3, 65]	×	11.0	44.8	14.9	15.4	36.8	16.7	27.8	12.1	1.8	31.2	3.4	<u>50.6</u>	12.6	36.7	12.5	21.87
P2RBox (2024) [2] [†]	×	<u>87.8</u>	<u>65.7</u>	<u>15.0</u>	60.7	<u>73.0</u>	<u>71.7</u>	<u>78.9</u>	81.5	44.5	<u>81.2</u>	41.2	39.3	<u>45.5</u>	<u>57.5</u>	<u>41.2</u>	<u>59.04</u>
PointOBB (2024) [33]	×	26.1	<u>65.7</u>	9.1	<u>59.4</u>	<u>65.8</u>	<u>34.9</u>	29.8	0.5	2.3	16.7	0.6	49.0	21.8	41.0	36.7	30.08
Point2RBox (2024) [66]	✓	62.9	64.3	14.4	35.0	28.2	38.9	33.3	25.2	2.2	44.5	3.4	48.1	25.9	45.0	22.6	34.07
Point2RBox+SK (2024) [66] [†]	✓	53.3	63.9	3.7	50.9	40.0	39.2	45.7	76.7	10.5	56.1	5.4	49.5	24.2	51.2	33.8	40.27
Point2RBox+SK (2024) [66] [†]	×	66.4	59.5	5.2	52.6	54.1	53.9	57.3	90.8	3.2	57.8	6.1	47.4	22.9	55.7	40.5	44.90
PointOBB-v2 (2025) [38]	×	64.5	27.8	1.9	36.2	58.8	47.2	53.4	<u>90.5</u>	62.2	45.3	12.1	41.7	8.1	43.7	32.0	41.68
PointOBB-v3 (2025) [67]	✓	30.9	39.4	13.5	22.7	61.2	7.0	43.1	62.4	59.8	47.3	2.7	45.1	16.8	55.2	11.4	41.29
PointOBB-v3 (2025) [67]	×	52.9	54.4	21.3	52.7	65.6	44.9	67.8	87.2	26.7	73.4	<u>32.6</u>	53.3	39.0	56.4	10.2	49.24
Point2RBox-v2 (ours)	✓	78.4	52.7	8.3	40.9	71.0	60.5	74.7	88.7	<u>65.5</u>	72.1	24.4	26.1	30.1	50.7	21.0	51.00
Point2RBox-v2 (ours)	×	88.0	72.6	8.0	46.2	79.6	76.3	86.9	89.1	79.7	82.9	26.2	45.3	45.8	66.3	46.3	62.61

*Comparison tracks: ✓ = End-to-end training and testing; × = Generating pseudo labels to train the FCOS detector (two-stage training).

[†]Using additional priors. P2RBox: Pre-trained SAM model; Point2RBox+SK: One-shot sketches for each class.

¹PL: Plane, BD: Baseball diamond, BR: Bridge, GTF: Ground track field, SV: Small vehicle, LV: Large vehicle, SH: Ship, TC: Tennis court, BC: Basketball court, ST: Storage tank, SBF: Soccer-ball field, RA: Roundabout, HA: Harbor, SP: Swimming pool, HC: Helicopter.

²-RBox: The minimum rectangle operation is performed on the output Mask to obtain the RBox.

Table 1. Detection performance of each category on the DOTA-v1.0 and the mean AP₅₀ of all categories.

Average precision (AP) is adopted as the primary metric. All the models are configured upon ResNet50 [13] and trained with AdamW [31]. **1) Learning rate.** Initialized at 5e-5, warm-up for 500 iterations, and divided by ten at each decay step. **2) Epochs.** 72 for HRSC; 12 for the others. **3) Augmentation.** Random rotation/flip for HRSC; random flip for the others. **4) Image size.** Split into 1,024 × 1,024 with an overlap of 200 for DOTA/FAIR1M/STAR; scaled to 800 × 800 for others. **5) Multi-scale.** All experiments evaluated without multi-scale technique [72]. **6) Datasets.** Six remote sensing and one retail scene datasets, covering all datasets used by the main counterparts [2, 33, 66]:

- **DOTA [48].** DOTA-v1.0 has 2,806 aerial images annotated with 15 categories, while DOTA-v1.5/2.0 are the extended versions with more small objects and categories.
- **DIOR [4].** It is an aerial image dataset re-annotated with RBoxes based on its original HBox version [18], with a high variation in object size and high intra-class diversity.
- **HRSC [30].** It contains ship instances on the sea and in-shore. The train/val/test set includes 436/181/444 images.
- **FAIR1M [40].** It has more than 1 million instances and more than 40,000 images for fine-grained object recognition in remote sensing imagery, annotated with 37 cate-

gories. The results are evaluated on FAIR1M-1.0.

- **STAR [22].** It is extensive for scene graph generation, covering more than 210,000 objects with diverse spatial resolutions, classified into 48 fine-grained categories and precisely annotated with oriented bounding boxes.
- **SKU110K [35].** It focuses on the detection of densely packed retail scenes with 110,712 objects in 11,762 images. The density reaches 86 instances per image.
- **RSAR [69].** It is a remote sensing dataset based on Synthetic Aperture Radar (SAR) imagery with 6 categories.

4.1. Main Results on DOTA-v1.0

Table 1 compares Point2RBox-v2 with the state-of-the-art methods, which can be categorized into two tracks:

1) End-to-end training. These methods apply the trained weakly-supervised detector directly to the test set. Without relying on priors, our approach demonstrates an improvement of 16.93% (51.00% vs. 34.07%) compared to Point2RBox. Even when compared to Point2RBox+SK, which incorporates additional data-side priors (i.e. one-shot examples for each class), our method still outperforms it by 10.73% (51.00% vs. 40.27%).

2) Two-stage training. These methods generate RBox

Methods	*	DOTA-v1.0	DOTA-v1.5	DOTA-v2.0	DIOR	HRSC	FAIR1M	STAR	SKU110K	RSAR
▼ <i>RBox-supervised OOD</i>										
RetinaNet (2017) [25]	✓	68.69	60.57	47.00	54.96	84.49	37.67	21.80	78.50	57.67
GWD (2021) [56]	✓	71.66	63.27	48.87	57.60	86.67	39.11	25.30	79.16	57.80
FCOS (2019) [42]	✓	72.44	64.53	51.77	59.83	88.99	41.25	28.10	80.09	66.66
S ² A-Net (2022) [12]	✓	75.81	66.53	52.39	61.41	90.10	42.44	27.30	80.36	66.47
▼ <i>HBox-supervised OOD</i>										
Sun et al. (2021) [41]	×	38.60	-	-	-	-	-	-	-	-
KCR (2023) [73]	✓	-	-	-	-	79.10	-	-	-	-
H2RBox (2023) [59]	✓	70.05	61.70	48.68	57.80	7.03	35.94	17.20	57.15	49.92
H2RBox-v2 (2023) [65]	✓	72.31	64.76	50.33	57.64	89.66	42.27	27.30	70.70	65.16
AFWS (2024) [32]	✓	72.55	65.92	51.73	59.07	-	41.80	-	-	-
▼ <i>Point-supervised OOD</i>										
P2RBox (2024) [2] [†]	×	<u>59.04</u>	-	-	-	-	-	-	-	-
PointSAM (2024) [27] [†]	×	-	-	-	46.20	-	-	-	-	-
PointOBB (2024) [33]	×	30.08	10.66	5.53	37.31	-	11.19	9.19	-	13.80
Point2RBox+SK (2024) [66] [†]	✓	40.27	30.51	23.43	27.34	79.40	20.03	7.86	3.41	27.81
PointOBB-v2 (2025) [38]	×	41.68	30.59	20.64	39.56	-	13.36	9.00	56.63	18.99
PointOBB-v3 (2025) [67]	✓	41.20	31.25	22.82	37.60	-	11.42	11.31	-	15.84
PointOBB-v3 (2025) [67]	×	49.24	33.79	23.52	40.18	-	18.35	<u>12.85</u>	-	22.60
Point2RBox-v2 (ours)	✓	51.00	<u>39.45</u>	<u>27.11</u>	34.70	<u>82.67</u>	<u>25.72</u>	7.80	<u>64.00</u>	<u>28.60</u>
Point2RBox-v2 (ours)	×	62.61	54.06	38.79	<u>44.45</u>	86.15	34.71	14.20	65.64	30.90

*Comparison tracks: ✓ = End-to-end training and testing; × = Generating pseudo labels to train the FCOS detector (two-stage training).

[†]Using additional priors. P2RBox/PointSAM: Pre-trained SAM model; Point2RBox+SK: One-shot sketches for each class.

Table 2. Accuracy (AP₅₀) comparisons on the DOTA-v1.0/1.5/2.0, DIOR, HRSC, FAIR1M, STAR, SKU110K, and RSAR datasets.

w_O	DOTA		HRSC	
	E2E	FCOS	E2E	FCOS
3	48.76	61.62	81.85	84.36
5	49.81	62.44	82.46	85.76
10	51.00	62.61	82.67	86.15
30	45.88	57.83	81.56	85.61

Table 3. Ablation with the weight of \mathcal{L}_O .

w_W	DOTA		HRSC	
	E2E	FCOS	E2E	FCOS
3	50.85	56.78	78.42	83.49
5	51.00	62.61	82.67	86.15
10	49.15	60.54	30.37	35.13
30	42.84	52.53	23.89	25.91

Table 4. Ablation with the weight of \mathcal{L}_W .

w_E	DOTA		HRSC	
	E2E	FCOS	E2E	FCOS
0.1	48.75	57.62	34.71	39.45
0.3	51.00	62.61	82.67	86.15
0.5	51.36	62.63	76.85	85.22
1.0	49.05	60.63	56.59	59.59

Table 5. Ablation with the weight of \mathcal{L}_E .

w_{ss}	DOTA		HRSC	
	E2E	FCOS	E2E	FCOS
0.1	49.28	59.66	73.66	78.92
1.0	51.00	62.61	82.67	86.15
3.0	49.15	59.20	1.30	1.65

Table 6. Ablation with the weight of \mathcal{L}_{ss} .

R / F / S	DOTA	HRSC	R / F / S	DOTA	HRSC
90% / 10% / 0%	60.42	85.46	80% / 20% / 0%	59.46	84.73
75% / 0% / 25%	60.79	86.22	60% / 15% / 25%	62.38	84.21
68% / 7% / 25%	62.61	86.15	38% / 37% / 25%	45.87	8.56
45% / 5% / 50%	60.55	85.34	40% / 10% / 50%	60.49	10.74

Table 7. Ablation with the proportion of augmented views in self-supervision.

labels on train/val sets, with which the FCOS detector is trained. In this two-stage mode, Point2RBox-v2 achieves an accuracy of 62.61%, considerably surpassing PointOBB series. Remarkably, it even outperforms the SAM-powered method P2RBox by 3.57% (62.61% vs. 59.04%).

Class-wise analysis. The FCOS detector trained with labels generated by Point2RBox-v2 achieves accuracy nearly equivalent to RBox-supervised FCOS across six high-density categories: SH (86.9% vs. 87.1%), SV (79.6% vs. 79.8%), LV (76.3% vs. 79.8%), PL (88.0% vs. 89.1%), ST (82.9% vs. 84.6%), and TC (89.1% vs. 90.4%). Interestingly, these six high-density categories account for 88% of DOTA instances. By annotating these categories with points and generating RBoxes using Point2RBox-v2 while labeling the other sparse categories with RBoxes, we can significantly reduce annotation labor without sacrificing much accuracy,

highlighting the valuable role our method can play.

4.2. Results on More Datasets

The results are displayed in Table 2. On more challenging DOTA-v1.5/2.0, Point2RBox-v2 presents a similar trend, 23.47%/18.15% higher than PointOBB-v2 in the pseudo-generation track. On the ship detection dataset HRSC, the gap between Point2RBox-v2 and RBox-supervised FCOS is only 2.84% (86.15% vs. 88.99%). DIOR is relatively sparse, leading to less improvement with our methods—lower than PointSAM (44.45% vs. 46.20%) but still higher than methods that do not use SAM. Our method also provides competitive performance on fine-grained datasets FAIR1M and STAR. In addition to remote sensing scenarios, we carry out experiments on SKU110K for densely packed retail scenes. Existing point-supervised methods struggle in this



Figure 5. Qualitative analysis on failed cases and overlap cases.

Modules					DOTA		HRSC	
\mathcal{L}_O	\mathcal{L}_W	\mathcal{L}_{ss}	\mathcal{L}_E	CP	E2E	FCOS	E2E	FCOS
✓					0.00	0.00	0.00	0.00
✓	✓				41.54	52.98	17.96	19.64
✓	✓	✓			46.64	54.26	18.10	22.13
✓	✓	✓	✓		49.55	61.88	78.79	83.79
✓	✓	✓	✓	✓	48.58	59.56	20.35	24.76
✓		✓	✓	✓	38.94	48.44	11.64	14.93
✓	✓	✓	✓	✓	47.08	55.05	19.58	21.78
✓	✓	✓	✓	✓	51.00	62.61	82.67	86.15

Table 8. Ablation with incremental addition of modules.

16	$K=24$	32	1.2	$\beta=1.6$	2.0
50.87	51.00	48.08	48.14	51.00	51.33

Table 9. Ablation with K and β in edge loss on DOTA (E2E).

σ	Point2RBox		PointOBB-v2		Point2RBox-v2	
	DOTA	HRSC	DOTA	HRSC	DOTA	HRSC
0%	40.27	79.40	44.85	-	62.61	86.15
10%	39.60	78.81	42.30	-	61.58	85.76
30%	38.42	78.28	38.46	-	60.31	85.71

Table 10. Ablation with the inaccuracy in point annotations.

case, whereas Point2RBox-v2 achieves performance on par with HBox-supervised H2RBox (65.64% vs. 57.15%).

4.3. Ablation Studies

Tables 3-10 display the ablation studies on DOTA-v1.0 and HRSC. ‘‘E2E’’ denotes end-to-end training; ‘‘FCOS’’ denotes two-stage training (i.e. generating pseudo labels to train FCOS). The final values adopted are highlighted in gray.

Weight of each loss. Tables 3-5 determine the weights of the proposed losses. Based on these experiments, the weights (w_O, w_W, w_E, w_{ss}) are set to (10, 5, 0.3, 1).

Proportion of augmented views. Table 7 studies the proportion between rotation, flip, and scale. The results are reported with two-stage training (FCOS). Based on the results, the proportion is set to 68%, 7%, and 25%.

Incremental addition of modules. Table 8 demonstrates the constraints from Gaussian and Voronoi achieve an accuracy of 52.98% on DOTA. Adding consistency loss and edge loss further boosts it to 54.26% and 61.88%, respectively, whereas the improvement from copy-paste is 0.73%. We also demonstrate the impact of omitting each core loss.

Edge loss parameters. We set $K = 24$ and $\beta = 1.6$ as they are observed to discern the correct edges during code development. Table 9 provides a more precise ablation.

Annotation inaccuracy. We offset the annotated points by a noise from the uniform distribution $[-\sigma H, +\sigma H]$, where H is the height of objects. Table 10 shows that the AP_{50} of Point2RBox-v2 decreases by less than 3% when noise is added to point annotations, demonstrating the robustness of the proposed learning mechanisms.

4.4. More Discussions

The qualitative analysis on the failed/overlap cases is shown in Fig. 5. **1) Failed cases.** Although our method performs well overall, it struggles with certain categories that are sparse and not constrained by other objects. **2) Overlap cases.** Minimizing overlap as a soft constraint during training does not entirely eliminate overlap. Once trained, the model remains robust to some overlap during inference.

5. Conclusion

This paper introduces Point2RBox-v2, a point-supervised oriented object detector that effectively leverages the arrangement and layout of instances. We propose the integration of Gaussian overlay and Voronoi tessellation to constrain the size and rotation of instances based on their spatial relationships. Additionally, by incorporating self-supervised consistency loss, edge loss, and copy-paste augmentation, the accuracy of the model is further enhanced.

Experiments yield the following observations: **1)** The integration of Gaussian and Voronoi concepts effectively harnesses the spatial layout of objects, significantly enhancing point-supervised OOD. **2)** Point2RBox-v2 demonstrates exceptional performance in densely packed scenes (see Fig. 2), where existing methods struggle. **3)** Our method does not require priors (i.e. pre-trained SAM or one-shot examples) and is applicable to both end-to-end and pseudo-generation modes. **4)** It advances the state of the art by a large amount, achieving 62.61%, 86.15%, and 34.71% on the DOTA-v1.0, HRSC, and FAIR1M datasets, respectively.

Limitations. The gap between Point2RBox-v2 and the RBox-supervised OOD is still huge in terms of sparse categories (i.e. BR/SBF) since little constraint can be obtained from the layout between them when the objects are sparse.

References

- [1] Franz Aurenhammer. Voronoi diagrams—a survey of a fundamental geometric data structure. *ACM Computing Surveys*, 23(3):345–405, 1991. 2, 4
- [2] Guangming Cao, Xuehui Yu, Wenwen Yu, Xumeng Han, Xue Yang, Guorong Li, Jianbin Jiao, and Zhenjun Han. P2rbox: Point prompt oriented object detection with SAM. *arXiv preprint arXiv:2311.13128*, 2024. 1, 2, 6, 7
- [3] Pengfei Chen, Xuehui Yu, Xumeng Han, Najmul Hassan, Kai Wang, Jiachen Li, Jian Zhao, Humphrey Shi, Zhenjun Han, and Qixiang Ye. Point-to-box network for accurate object detection via single point supervision. In *European Conference on Computer Vision*, 2022. 3, 6
- [4] Gong Cheng, Jiabao Wang, Ke Li, Xingxing Xie, Chunbo Lang, Yanqing Yao, and Junwei Han. Anchor-free oriented proposal generator for object detection. *IEEE Transactions on Geoscience and Remote Sensing*, 2022. 6
- [5] Jian Ding, Nan Xue, Yang Long, Gui-Song Xia, and Qikai Lu. Learning roi transformer for oriented object detection in aerial images. In *IEEE/CVF Conference on Computer Vision and Pattern Recognition*, pages 2849–2858, 2019. 2
- [6] Di Feng, Christian Haase-Schütz, Lars Rosenbaum, Heinz Hertlein, Claudius Gläser, Fabian Timm, Werner Wiesbeck, and Klaus Dietmayer. Deep multi-modal object detection and semantic segmentation for autonomous driving: Datasets, methods, and challenges. *IEEE Transactions on Intelligent Transportation Systems*, 22(3):1341–1360, 2021. 1
- [7] Kun Fu, Zhonghan Chang, Yue Zhang, Guanguan Xu, Keshu Zhang, and Xian Sun. Rotation-aware and multi-scale convolutional neural network for object detection in remote sensing images. *ISPRS Journal of Photogrammetry and Remote Sensing*, 161:294–308, 2020. 1
- [8] Shuyong Gao, Wei Zhang, Yan Wang, Qianyu Guo, Chenglong Zhang, Yangji He, and Wenqiang Zhang. Weakly-supervised salient object detection using point supervision. In *AAAI Conference on Artificial Intelligence*, pages 670–678, 2022. 3
- [9] Golnaz Ghiasi, Yin Cui, Aravind Srinivas, Rui Qian, Tsung-Yi Lin, Ekin D. Cubuk, Quoc V. Le, and Barret Zoph. Simple copy-paste is a strong data augmentation method for instance segmentation. In *IEEE/CVF Conference on Computer Vision and Pattern Recognition*, pages 2918–2928, 2021. 5
- [10] Eran Goldman, Roei Herzig, Aviv Eisenschtat, Jacob Goldberg, and Tal Hassner. Precise detection in densely packed scenes. In *IEEE/CVF Conference on Computer Vision and Pattern Recognition*, pages 5227–5236, 2019. 1
- [11] Jiaming Han, Jian Ding, Nan Xue, and Gui-Song Xia. Redet: A rotation-equivariant detector for aerial object detection. In *IEEE/CVF Conference on Computer Vision and Pattern Recognition*, pages 2785–2794, 2021. 2
- [12] Jiaming Han, Jian Ding, Jie Li, and Gui-Song Xia. Align deep features for oriented object detection. *IEEE Transactions on Geoscience and Remote Sensing*, 60:1–11, 2022. 2, 6, 7
- [13] Kaiming He, Xiangyu Zhang, Shaoqing Ren, and Jian Sun. Deep residual learning for image recognition. In *IEEE Conference on Computer Vision and Pattern Recognition*, pages 770–778, 2016. 3, 6
- [14] Kaiming He, Georgia Gkioxari, Piotr Dollar, and Ross Girshick. Mask r-cnn. In *IEEE International Conference on Computer Vision*, 2017. 5
- [15] Liping Hou, Ke Lu, Xue Yang, Yuqiu Li, and Jian Xue. G-rep: Gaussian representation for arbitrary-oriented object detection. *Remote Sensing*, 15(3):757, 2023. 2
- [16] Javed Iqbal, Muhammad Akhtar Munir, Arif Mahmood, Afshen Rafaqat Ali, and Mohsen Ali. Leveraging orientation for weakly supervised object detection with application to firearm localization. *Neurocomputing*, 440:310–320, 2021. 3
- [17] Alexander Kirillov, Eric Mintun, Nikhila Ravi, Hanzi Mao, Chloe Rolland, Laura Gustafson, Tete Xiao, Spencer Whitehead, Alexander C Berg, Wan-Yen Lo, et al. Segment anything. In *IEEE/CVF International Conference on Computer Vision*, pages 4015–4026, 2023. 1, 3
- [18] Ke Li, Gang Wan, Gong Cheng, Liqiu Meng, and Junwei Han. Object detection in optical remote sensing images: A survey and a new benchmark. *ISPRS Journal of Photogrammetry and Remote Sensing*, 159:296–307, 2020. 6
- [19] Qingyun Li, Yushi Chen, Xinya Shu, Dong Chen, Xin He, Yi Yu, and Xue Yang. A simple aerial detection baseline of multimodal language models. *arXiv preprint arXiv:2501.09720*, 2025. 2
- [20] Wentong Li, Yijie Chen, Kaixuan Hu, and Jianke Zhu. Oriented reppoints for aerial object detection. In *IEEE/CVF Conference on Computer Vision and Pattern Recognition*, pages 1829–1838, 2022. 2
- [21] Wentong Li, Yuqian Yuan, Song Wang, Jianke Zhu, Jianshu Li, Jian Liu, and Lei Zhang. Point2mask: Point-supervised panoptic segmentation via optimal transport. In *IEEE International Conference on Computer Vision*, 2023. 2, 3, 6
- [22] Yansheng Li, Linlin Wang, Tingzhu Wang, Xue Yang, Junwei Luo, Qi Wang, Youming Deng, Wenbin Wang, Xian Sun, Haifeng Li, Bo Dang, Yongjun Zhang, Yi Yu, and Yan Junchi. Star: A first-ever dataset and a large-scale benchmark for scene graph generation in large-size satellite imagery. *arXiv preprint arXiv:2406.09410*, 2024. 6
- [23] Minghui Liao, Zhen Zhu, Baoguang Shi, Gui-Song Xia, and Xiang Bai. Rotation-sensitive regression for oriented scene text detection. In *IEEE/CVF Conference on Computer Vision and Pattern Recognition*, pages 5909–5918, 2018. 1
- [24] Tsung-Yi Lin, Piotr Dollár, Ross Girshick, Kaiming He, Bharath Hariharan, and Serge Belongie. Feature pyramid networks for object detection. In *IEEE Conference on Computer Vision and Pattern Recognition*, pages 2117–2125, 2017. 3
- [25] Tsung-Yi Lin, Priya Goyal, Ross Girshick, Kaiming He, and Piotr Dollár. Focal loss for dense object detection. *IEEE Transactions on Pattern Analysis and Machine Intelligence*, 42(2):318–327, 2020. 2, 5, 6, 7
- [26] Li Liu, Wanli Ouyang, Xiaogang Wang, Paul Fieguth, Jie Chen, Xinwang Liu, and Matti Pietikäinen. Deep learning for generic object detection: A survey. *International Journal of Computer Vision*, 128(2):261–318, 2020. 2

- [27] Nanqing Liu, Xun Xu, Yongyi Su, Haojie Zhang, and Heng-Chao Li. Pointsam: Pointly-supervised segment anything model for remote sensing images. *arXiv preprint arXiv:2409.13401*, 2024. 1, 2, 7
- [28] Xuebo Liu, Ding Liang, Shi Yan, Dagui Chen, Yu Qiao, and Junjie Yan. Fots: Fast oriented text spotting with a unified network. In *IEEE/CVF Conference on Computer Vision and Pattern Recognition*, pages 5676–5685, 2018. 1
- [29] Yuekai Liu, Hongli Gao, Liang Guo, Aoping Qin, Canyu Cai, and Zhichao You. A data-flow oriented deep ensemble learning method for real-time surface defect inspection. *IEEE Transactions on Instrumentation and Measurement*, 69(7): 4681–4691, 2020. 1
- [30] Zikun Liu, Liu Yuan, Lubin Weng, and Yiping Yang. A high resolution optical satellite image dataset for ship recognition and some new baselines. In *International Conference on Pattern Recognition Applications and Methods*, pages 324–331, 2017. 1, 6
- [31] Ilya Loshchilov and Frank Hutter. Decoupled weight decay regularization. In *International Conference on Learning Representations*, 2018. 6
- [32] Junyan Lu, Qinglei Hu, Ruifei Zhu, Yali Wei, and Tie Li. Afws: Angle-free weakly-supervised rotating object detection for remote sensing images. *IEEE Transactions on Geoscience and Remote Sensing*, 2024. 7
- [33] Junwei Luo, Xue Yang, Yi Yu, Qingyun Li, Junchi Yan, and Yansheng Li. Pointobb: Learning oriented object detection via single point supervision. In *IEEE/CVF Conference on Computer Vision and Pattern Recognition*, 2024. 1, 2, 3, 6, 7
- [34] Jeffri Murugarra-Llerena, Lucas N Kirsten, Luis Felipe Zeni, and Claudio R Jung. Probabilistic intersection-over-union for training and evaluation of oriented object detectors. *IEEE Transactions on Image Processing*, 2024. 2
- [35] Xingjia Pan, Yuqiang Ren, Kekai Sheng, Weiming Dong, Haolei Yuan, Xiaowei Guo, Chongyang Ma, and Changsheng Xu. Dynamic refinement network for oriented and densely packed object detection. In *IEEE/CVF Conference on Computer Vision and Pattern Recognition*, pages 11207–11216, 2020. 1, 6
- [36] Adam Paszke, Sam Gross, Francisco Massa, Adam Lerer, James Bradbury, Gregory Chanan, Trevor Killeen, Zeming Lin, Natalia Gimelshein, Luca Antiga, Alban Desmaison, Andreas Kopf, Edward Yang, Zachary DeVito, Martin Raison, Alykhan Tejani, Sasank Chilamkurthy, Benoit Steiner, Lu Fang, Junjie Bai, and Soumith Chintala. Pytorch: An imperative style, high-performance deep learning library. In *Advances in Neural Information Processing Systems*, pages 8024–8035, 2019. 5
- [37] Wen Qian, Xue Yang, Silong Peng, Junchi Yan, and Yue Guo. Learning modulated loss for rotated object detection. In *AAAI Conference on Artificial Intelligence*, pages 2458–2466, 2021. 2
- [38] Botao Ren, Xue Yang, Yi Yu, Junwei Luo, and Zhidong Deng. Pointobb-v2: Towards simpler, faster, and stronger single point supervised oriented object detection. In *International Conference on Learning Representations*, 2025. 1, 2, 3, 6, 7
- [39] Xavier Soria, Yachuan Li, Mohammad Rouhani, and Angel D. Sappa. Tiny and efficient model for the edge detection generalization. In *IEEE/CVF International Conference on Computer Vision Workshops*, pages 1364–1373, 2023. 5
- [40] Xian Sun, Peijin Wang, Zhiyuan Yan, Feng Xu, Ruiping Wang, Wenhui Diao, Jin Chen, Jihao Li, Yingchao Feng, Tao Xu, Martin Weinmann, Stefan Hinz, Cheng Wang, and Kun Fu. Fair1m: A benchmark dataset for fine-grained object recognition in high-resolution remote sensing imagery. *ISPRS Journal of Photogrammetry and Remote Sensing*, 184:116–130, 2022. 6
- [41] Yongqing Sun, Jie Ran, Feng Yang, Chenqiang Gao, Takayuki Kurozumi, Hideaki Kimata, and Ziqi Ye. Oriented object detection for remote sensing images based on weakly supervised learning. In *IEEE International Conference on Multimedia & Expo Workshops*, pages 1–6, 2021. 3, 6, 7
- [42] Zhi Tian, Chunhua Shen, Hao Chen, and Tong He. Fcos: Fully convolutional one-stage object detection. In *IEEE/CVF International Conference on Computer Vision*, pages 9626–9635, 2019. 2, 6, 7
- [43] Zhi Tian, Chunhua Shen, Xinlong Wang, and Hao Chen. Boxinst: High-performance instance segmentation with box annotations. In *IEEE/CVF Conference on Computer Vision and Pattern Recognition*, pages 5443–5452, 2021. 6
- [44] L. Vincent and P. Soille. Watersheds in digital spaces: an efficient algorithm based on immersion simulations. *IEEE Transactions on Pattern Analysis and Machine Intelligence*, 13(6):583–598, 1991. 4
- [45] Linfei Wang, Yibing Zhan, Xu Lin, Baosheng Yu, Liang Ding, Jianqing Zhu, and Dapeng Tao. Explicit and implicit box equivariance learning for weakly-supervised rotated object detection. *IEEE Transactions on Emerging Topics in Computational Intelligence*, 2024. 3, 6
- [46] Long Wen, Yu Cheng, Yi Fang, and Xinyu Li. A comprehensive survey of oriented object detection in remote sensing images. *Expert Systems with Applications*, page 119960, 2023. 2
- [47] Hongjin Wu, Ruoshan Lei, and Yibing Peng. Pcbnet: A lightweight convolutional neural network for defect inspection in surface mount technology. *IEEE Transactions on Instrumentation and Measurement*, 71:1–14, 2022. 1
- [48] Gui-Song Xia, Xiang Bai, Jian Ding, Zhen Zhu, Serge Belongie, Jiebo Luo, Mihai Datcu, Marcello Pelillo, and Liangpei Zhang. Dota: A large-scale dataset for object detection in aerial images. In *IEEE Conference on Computer Vision and Pattern Recognition*, pages 3974–3983, 2018. 1, 6
- [49] Xingxing Xie, Gong Cheng, Jiabao Wang, Xiwen Yao, and Junwei Han. Oriented r-cnn for object detection. In *IEEE/CVF International Conference on Computer Vision*, pages 3520–3529, 2021. 2
- [50] Xue Yang and Junchi Yan. Arbitrary-oriented object detection with circular smooth label. In *European Conference on Computer Vision*, pages 677–694, 2020. 2
- [51] Xue Yang and Junchi Yan. On the arbitrary-oriented object detection: Classification based approaches revisited. *International Journal of Computer Vision*, 130(5):1340–1365, 2022. 1, 2
- [52] Xue Yang, Hao Sun, Kun Fu, Jirui Yang, Xian Sun, Menglong Yan, and Zhi Guo. Automatic ship detection in remote

- sensing images from google earth of complex scenes based on multiscale rotation dense feature pyramid networks. *Remote sensing*, 10(1):132, 2018. 1, 2
- [53] Xue Yang, Jirui Yang, Junchi Yan, Yue Zhang, Tengfei Zhang, Zhi Guo, Xian Sun, and Kun Fu. Scrdet: Towards more robust detection for small, cluttered and rotated objects. In *IEEE/CVF International Conference on Computer Vision*, pages 8231–8240, 2019. 2
- [54] Xue Yang, Liping Hou, Yue Zhou, Wentao Wang, and Junchi Yan. Dense label encoding for boundary discontinuity free rotation detection. In *IEEE/CVF Conference on Computer Vision and Pattern Recognition*, pages 15814–15824, 2021. 2
- [55] Xue Yang, Junchi Yan, Ziming Feng, and Tao He. R3det: Refined single-stage detector with feature refinement for rotating object. In *AAAI Conference on Artificial Intelligence*, pages 3163–3171, 2021. 2
- [56] Xue Yang, Junchi Yan, Ming Qi, Wentao Wang, Xiaopeng Zhang, and Tian Qi. Rethinking rotated object detection with gaussian wasserstein distance loss. In *38th International Conference on Machine Learning*, pages 11830–11841, 2021. 2, 6, 7
- [57] Xue Yang, Xiaojiang Yang, Jirui Yang, Qi Ming, Wentao Wang, Qi Tian, and Junchi Yan. Learning high-precision bounding box for rotated object detection via kullback-leibler divergence. In *Advances in Neural Information Processing Systems*, pages 18381–18394, 2021. 2
- [58] Xue Yang, Junchi Yan, Wenlong Liao, Xiaokang Yang, Jin Tang, and Tao He. Scrdet++: Detecting small, cluttered and rotated objects via instance-level feature denoising and rotation loss smoothing. *IEEE Transactions on Pattern Analysis and Machine Intelligence*, 45(2):2384–2399, 2022. 2
- [59] Xue Yang, Gefan Zhang, Wentong Li, Xuehui Wang, Yue Zhou, and Junchi Yan. H2rbox: Horizontal box annotation is all you need for oriented object detection. *International Conference on Learning Representations*, 2023. 1, 3, 6, 7
- [60] Xue Yang, Gefan Zhang, Xiaojiang Yang, Yue Zhou, Wentao Wang, Jin Tang, Tao He, and Junchi Yan. Detecting rotated objects as gaussian distributions and its 3-d generalization. *IEEE Transactions on Pattern Analysis and Machine Intelligence*, 45(4):4335–4354, 2023. 2, 3, 4, 5
- [61] Xue Yang, Yue Zhou, Gefan Zhang, Jirui Yang, Wentao Wang, Junchi Yan, Xiaopeng Zhang, and Qi Tian. The kfiou loss for rotated object detection. In *International Conference on Learning Representations*, 2023. 2
- [62] Ze Yang, Shaohui Liu, Han Hu, Liwei Wang, and Stephen Lin. Reppoints: Point set representation for object detection. In *IEEE/CVF International Conference on Computer Vision*, pages 9656–9665, 2019. 2, 6
- [63] Yi Yu and Feipeng Da. Phase-shifting coder: Predicting accurate orientation in oriented object detection. In *IEEE/CVF Conference on Computer Vision and Pattern Recognition*, 2023. 2
- [64] Yi Yu and Feipeng Da. On boundary discontinuity in angle regression based arbitrary oriented object detection. *IEEE Transactions on Pattern Analysis and Machine Intelligence*, pages 1–14, 2024. 3
- [65] Yi Yu, Xue Yang, Qingyun Li, Yue Zhou, Feipeng Da, and Junchi Yan. H2rbox-v2: Incorporating symmetry for boosting horizontal box supervised oriented object detection. In *Advances in Neural Information Processing Systems*, 2023. 1, 3, 5, 6, 7
- [66] Yi Yu, Xue Yang, Qingyun Li, Feipeng Da, Jifeng Dai, Yu Qiao, and Junchi Yan. Point2rbox: Combine knowledge from synthetic visual patterns for end-to-end oriented object detection with single point supervision. In *IEEE/CVF Conference on Computer Vision and Pattern Recognition*, 2024. 1, 2, 3, 6, 7
- [67] Peiyuan Zhang, Junwei Luo, Xue Yang, Yi Yu, Qingyun Li, Yue Zhou, Xiaosong Jia, Xudong Lu, Jingdong Chen, Xiang Li, et al. Pointobb-v3: Expanding performance boundaries of single point-supervised oriented object detection. *arXiv preprint arXiv:2501.13898*, 2025. 1, 2, 3, 6, 7
- [68] Shun Zhang, Jihui Long, Yaohui Xu, and Shaohui Mei. Pmho: Point-supervised oriented object detection based on segmentation-driven proposal generation. *IEEE Transactions on Geoscience and Remote Sensing*, 2024. 1, 2
- [69] Xin Zhang, Xue Yang, Yuxuan Li, Jian Yang, Ming-Ming Cheng, and Xiang Li. Rsar: Restricted state angle resolver and rotated sar benchmark. *arXiv preprint arXiv:2501.04440*, 2025. 6
- [70] Zhong-Qiu Zhao, Peng Zheng, Shou-Tao Xu, and Xindong Wu. Object detection with deep learning: A review. *IEEE Transactions on Neural Networks and Learning Systems*, 30(11):3212–3232, 2019. 2
- [71] Xinyu Zhou, Cong Yao, He Wen, Yuzhi Wang, Shuchang Zhou, Weiran He, and Jiajun Liang. East: An efficient and accurate scene text detector. In *IEEE Conference on Computer Vision and Pattern Recognition*, pages 2642–2651, 2017. 1
- [72] Yue Zhou, Xue Yang, Gefan Zhang, Jiabao Wang, Yanyi Liu, Liping Hou, Xue Jiang, Xingzhao Liu, Junchi Yan, Chengqi Lyu, et al. Mmrotate: A rotated object detection benchmark using pytorch. In *30th ACM International Conference on Multimedia*, pages 7331–7334, 2022. 5, 6
- [73] Tianyu Zhu, Bryce Ferenczi, Pulak Purkait, Tom Drummond, Hamid Rezaatofghi, and Anton van den Hengel. Knowledge combination to learn rotated detection without rotated annotation. In *IEEE/CVF Conference on Computer Vision and Pattern Recognition*, 2023. 3, 7